



Contents lists available at ScienceDirect

Journal of the Mechanics and Physics of Solids

journal homepage: www.elsevier.com/locate/jmps

Intrinsic stress mitigation via elastic softening during two-step electrochemical lithiation of amorphous silicon



Zheng Jia, Teng Li*

Department of Mechanical Engineering, University of Maryland, College Park, MD 20742, USA

ARTICLE INFO

Article history:

Received 9 October 2015

Received in revised form

15 March 2016

Accepted 19 March 2016

Available online 28 March 2016

Keywords:

Amorphous silicon

Two-step lithiation

Chemo-mechanical modeling

Fracture

Lithium-ion battery

Anode

ABSTRACT

Recent experiments and first-principles calculations show the two-step lithiation of amorphous silicon (a-Si). In the first step, the lithiation progresses by the movement of a sharp phase boundary between a pristine a-Si phase and an intermediate Li_7Si phase until the a-Si phase is fully consumed. Then the second step sets in without a visible interface, with the Li_7Si phase continuously lithiating to a $\text{Li}_{3.75}\text{Si}$ phase. This unique feature of lithiation is believed to have important consequences for mechanical durability of a-Si anodes in lithium ion batteries, however the mechanistic understanding of such consequences is still elusive so far. Here, we reveal an intrinsic stress mitigation mechanism due to elastic softening during two-step lithiation of a-Si, via chemo-mechanical modeling. We find that lithiation-induced elastic softening of a-Si leads to effective stress mitigation in the second step of lithiation. These mechanistic findings allow for the first time to quantitatively predict the critical size of an a-Si anode below which the anode becomes immune to lithiation-induced fracture, which is in good agreement with experimental observations. Further studies on lithiation kinetics suggest that the two-step lithiation also results in a lower stress-induced energy barrier for lithiation. The present study reveals the physical underpinnings of previously unexplained favorable lithiation kinetics and fracture behavior of a-Si anodes, and thus sheds light on quantitative design guidelines toward high-performance anodes for lithium ion batteries.

© 2016 Elsevier Ltd. All rights reserved.

1. Introduction

There are surging interests recently in exploring new high-capacity anode materials for next-generation high-performance lithium ion batteries (Armand and Tarascon, 2008; Tarascon and Armand, 2001; Yang et al., 2010). Silicon is emerging as the most promising anode material, given its theoretical capacity as high as ten times as that of conventional graphite-based anodes (Li and Dahn, 2007; Obrovac and Christensen, 2004; Wu and Cui, 2012). However, the large volume change ($\sim 300\%$) during lithium insertion/extraction may fracture the active silicon anodes and solid-electrolyte interface (Wang et al., 2015; Zhao et al., 2012a), resulting in irreversible capacity fading (Chan et al., 2008; Liu et al., 2011, 2012c). Intensive research efforts have been focused on mitigating lithiation-induced mechanical failure of anodes by developing nanostructured anodes, e.g., nanowires (Bogart et al., 2014; Chan et al., 2008; Karki et al., 2012; Lee et al., 2015), nano-sized thin films (Takamura et al., 2004), nanoporous structures (Baggetto et al., 2011; Kim et al., 2008; Liu et al., 2013; Lu et al., 2015),

* Corresponding author.

E-mail address: lit@umd.edu (T. Li).

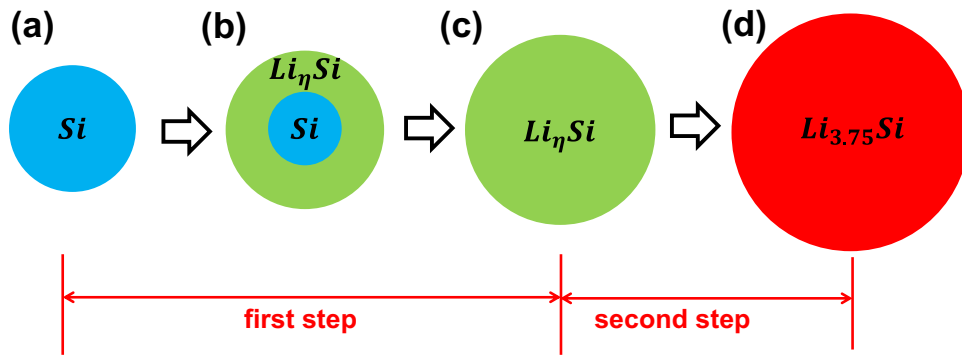


Fig. 1. Schematic of the two-step lithiation of an a-Si nanoparticle anode. In the first steps (a)–(c), the lithiation advances by a two-phase mechanism with a sharp amorphous–amorphous interface between the a-Si phase and the Li_ηSi phase migrating inward until the a-Si phase is fully consumed, resulting in a nanoparticle in Li_ηSi phase. In the second step (c) and (d), the Li_ηSi phase further lithiates to a $\text{Li}_{3.75}\text{Si}$ phase without a visible interface. The value of intermediate lithiation level η is estimated to be 2.5 by in situ TEM observation and be 2 by ab initio calculations.

nanoparticles (Chen et al., 2015; Haftbaradaran et al., 2012; Lu et al., 2015; Soni et al., 2012; Xu and Zhao, 2015) and nanowalls (Wan et al., 2014). The success of developing high performance silicon-based anodes hinges upon the fundamental understanding of lithiation mechanism, which in turn strongly affects the associated stress evolution, fracture behavior and lithiation kinetics of such anodes (Cui et al., 2013b; Gu et al., 2014; Jia and Li, 2015; Luo et al., 2015; Yang et al., 2015). Significant progress aside, the existing mechanistic understanding in these regards is far from being mature.

Recent in situ transmission electron microscope (TEM) studies show that the lithiation of crystalline silicon (c-Si) advances by the movement of an atomically sharp reaction front, which separates a pristine c-Si phase and an amorphous $\text{Li}_{3.75}\text{Si}$ phase. In other words, the lithiation of c-Si occurs through a two-phase reaction (Goldman et al., 2011; Key et al., 2009, 2011; Lee et al., 2011; Liu et al., 2012b; McDowell et al., 2013b; Zhu, 2015). A drastic change of Li concentration across the amorphous–crystalline phase boundary results in significant volume mismatch, causing high stress and possible mechanical failure of the anodes. Moreover, it is shown that lithiation of c-Si is highly anisotropic, with predominant volume expansion along $\langle 110 \rangle$ direction but negligibly small expansion along $\langle 111 \rangle$ direction, so that the fracture of c-Si anodes are preferentially located between neighboring $\langle 110 \rangle$ planes (Lee et al., 2012; Liu et al., 2011; Pharr et al., 2012). This intriguing fracture behavior is attributed to the intensified tensile hoop stress induced by the anisotropic volume expansion during lithiation of c-Si.

Motivated by the needs to alleviate severe stress induced by anisotropic lithiation of c-Si anode, considerable efforts have been devoted to designing amorphous silicon (a-Si) anodes, which is intuitively thought to be lithiated via one-phase mechanism and thus has less heterogeneous volume expansion. Surprisingly, recent in situ TEM and first-principles calculations reveal that the lithiation of a-Si indeed occurs in a two-step process (Cubuk and Kaxiras, 2014; McDowell et al., 2013a; Wang et al., 2013), as depicted in Fig. 1. In the first step, the lithiation advances by a two-phase mechanism with a migrating amorphous–amorphous interface between a-Si phase and an intermediate Li_ηSi phase until the a-Si phase is fully consumed. Then the second step of lithiation sets in without any visible electrochemical reaction interface, resulting in the final product of $\text{Li}_{3.75}\text{Si}$ with a total volume expansion of $\sim 280\%$ (Sun et al., 2013; Wang et al., 2013). The value of the intermediate lithiation level η has not been conclusively determined yet. It is estimated to be 2.5 based on in situ TEM observations (Wang et al., 2013), while first-principles calculations predict that the critical structural change between two steps occurs around $\eta \approx 2$ (Cubuk and Kaxiras, 2014). Without losing generality, in this study, the intermediate lithiation phase is taken to be $\text{Li}_{2.5}\text{Si}$, with η being 2.5. Fracture mechanics study dictates that there exists a critical size of nanoparticle silicon anodes, above which the anode fractures during charging/discharging and below which the anode is immune from the lithiation-induced fracture. Recent experiments show that such a critical size of a-Si anodes is larger than that of its c-Si counterparts (Berla et al., 2014; McDowell et al., 2013a). While existing progress on developing a-Si anodes is encouraging, fundamental understanding of the stress evolution during lithiation of a-Si, and particularly, the underlying mechanism of stress mitigation by the two-step lithiation of a-Si anodes are highly desirable for optimal anode design but still remain elusive so far.

In this work, we report a systematic mechanistic study of the two-step lithiation and the concurrent stress evolution in a-Si nanoparticle anodes via chemo-mechanical modeling. Our case studies on both solid and hollow a-Si nanoparticle anodes reveal that lithiation-induced elastic softening of a-Si leads to effective stress mitigation in the second step of lithiation. We report a fracture mechanics model that allows for quantitative prediction of the critical sizes of a-Si and c-Si nanoparticle anodes, in agreement with experimental observations. Further studies on lithiation kinetics suggest that the two-step lithiation results in a lower stress-induced energy barrier for lithiation than that in the one-step lithiation. The mechanistic findings from the present study can offer quantitative insights in optimal design guidelines toward high-performance a-Si anodes. Given that the two-step charging also occurs in electrodes in other battery systems (e.g., tin anodes in sodium-ion batteries) in a similar fashion (Wang et al., 2012), the present model thus can potentially shed light on developing a class of new anode materials for advanced battery technology.

The structure of the article is organized as follows. Section 2 describes a chemo-mechanical model for the two-step lithiation process of an a-Si particle. Section 3 reports numerical and analytical results on the stress generation and mitigation in an a-Si particle under two-step lithiation. The influence of the intrinsic stress mitigation mechanism and lithiation kinetics of the a-Si particle are discussed in Section 4 and Section 5, respectively. Conclusions are given in Section 6.

2. A chemo-mechanical modeling scheme for two-step lithiation

Recent first-principles calculations predict that, during the second step of lithiation, the lithiated anode always stays in the same structural phase Li_xSi with a uniform lithium concentration (Cubuk and Kaxiras, 2014), indicating a homogeneous volume expansion during the second step. In contrast to highly anisotropic lithiation of c-Si, lithiation of a-Si is rather isotropic (McDowell et al., 2013a). First-principles calculations also reveal that Young's modulus and Poisson's ratio of lithiated silicon both decrease with increasing Li concentration from 160 to 40 GPa and from 0.24 to 0.22 in a linear manner (Shenoy et al., 2010; Yang et al., 2012; Zhao et al., 2011). As to be shown later, such lithiation-induced elastic softening significantly affects the stress evolution in a-Si during lithiation and plays a pivotal role in dictating the lithiation kinetics and fracture behavior of a-Si anode.

Inspired by the in situ TEM observations and results from first-principles calculations, we develop a chemo-mechanical modeling scheme to simulate the two-step lithiation of a-Si nanoparticles and the concurrent stress evolution, using commercial finite element method package ABAQUS 6.13. In order to mimic the migration of the amorphous–amorphous interface in the first step of lithiation, a spherical a-Si particle model is evenly divided into N number of shells, where N

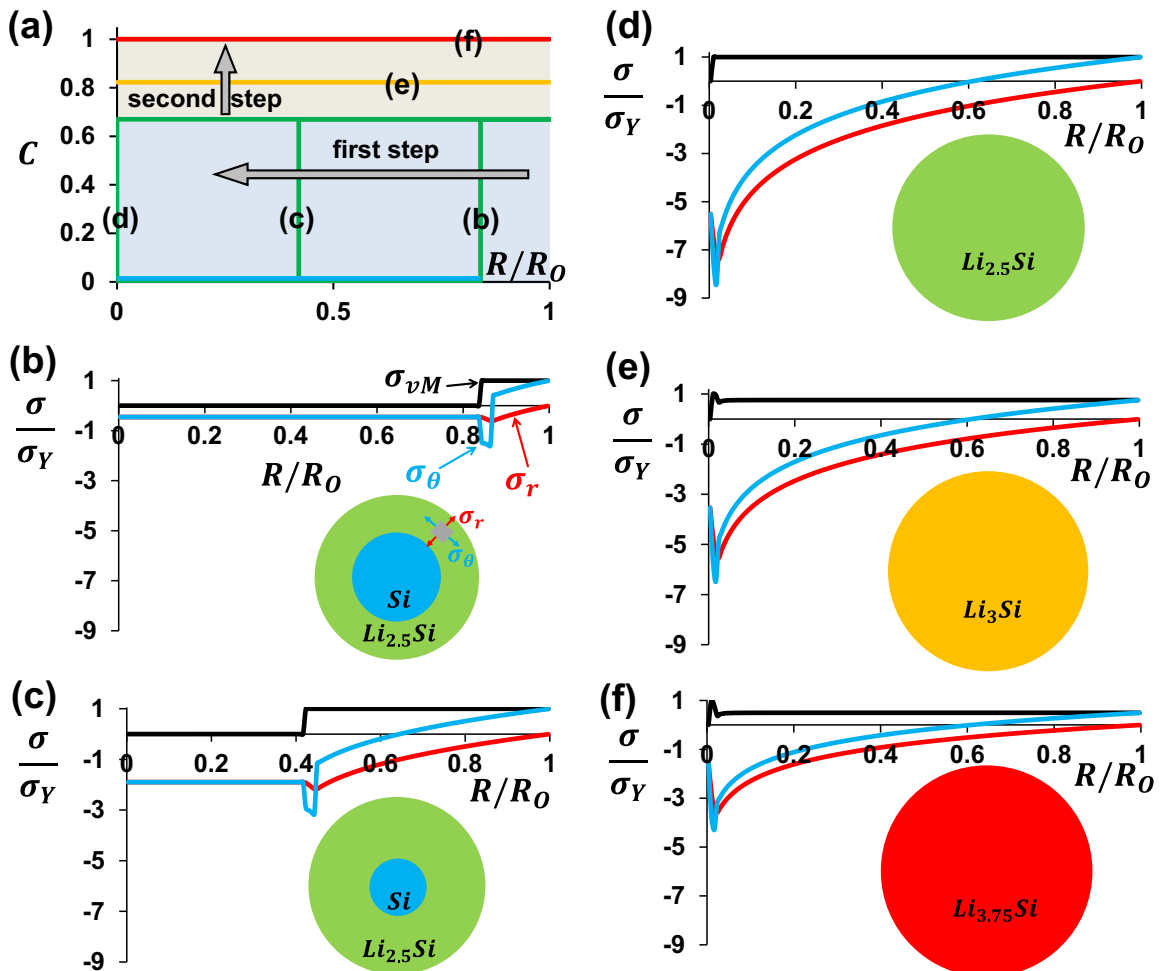


Fig. 2. Evolution of lithium concentration and resulting stresses in an a-Si particle during the two-step lithiation. (a) Radial distribution of normalized lithium concentration C at five representative stages during the two-step lithiation. The first step of lithiation advances via a two-phase mechanism, with a sharp a-Si/ $\text{Li}_{2.5}\text{Si}$ interface migrating inward. In the second step, the lithium concentration distribution within the particle is uniform and ramps up from 0.67 ($\text{Li}_{2.5}\text{Si}$) to 1 ($\text{Li}_{3.75}\text{Si}$). The corresponding stress distributions (σ_{vM} , σ_θ , σ_r) in the first step of lithiation (b) and (d) and stress distributions in the second step of lithiation (e) and (f) are given with illustrations showing the phases within the particles.

denotes an integer which takes a value between 50 and 100, depending on the particle size. In the simulation, these shells are sequentially lithiated one by one from outer ones to inner ones by prescribing a normalized concentration $C = 0.67$ on each shell sequentially (C is defined by $C = \frac{x}{3.75}$ for any phase of Li_xSi ; namely, $C = 0$ represents a-Si phase, while $C = 1$ the $\text{Li}_{3.75}\text{Si}$ phase), which is corresponding to the $\text{Li}_{2.5}\text{Si}$ phase. Experimental evidence on c-Si has accumulated that the reaction front is atomically sharp with a thickness of ~ 1 nm (Liu et al., 2012b). In our simulation on a-Si, the thickness of the amorphous–amorphous interface is determined by the thickness of each shell, which is set to be 2 nm to make a compromise between numerical expense and simulation accuracy. The second-step lithiation of a-Si is homogeneous with zero gradients of lithium concentration within a-Si particles (Cubuk and Kaxiras, 2014). Therefore, in the simulation, during the second step of lithiation, the normalized lithium concentration C is taken to be spatially uniform within the lithiated silicon particle and ramps from 0.67 to 1 as the second step of lithiation proceeds.

The large and permanent deformation driven by the two-step lithiation can be described by a rate-form finite-strain plasticity theory, in which the deformation is characterized by the stretch rate tensor \mathbf{D} . The total stretch rate tensor \mathbf{D} of lithiated silicon can be expressed as

$$\mathbf{D} = \mathbf{D}^P + \mathbf{D}^E + \mathbf{D}^L, \quad (1)$$

where \mathbf{D}^P , \mathbf{D}^E , \mathbf{D}^L are the plastic, elastic and lithiation-induced volumetric parts of stretch rate tensor, respectively. The lithiation-induced volumetric stretch rate \mathbf{D}^L is dilational and proportional to the rate of the normalized lithium concentration \dot{C} , i.e., $\mathbf{D}^L = \beta \dot{C} \mathbf{I}$. Here, β is the lithiation-induced volume expansion coefficient which is analogous to thermal expansion coefficient and it is taken to be 0.6 to model the 300% volume change at full lithiation (Wang et al., 2013). \mathbf{I} is the identity tensor. The lithiated Li_xSi ($0 < x \leq 3.75$) phase is considered to be linear-elastic and perfectly-plastic. Specifically, the rate of stress measure can be related to the elastic stretch rate tensor by (Bower et al., 2011; Yang et al., 2014)

$$\dot{\boldsymbol{\tau}}^v = \frac{E_{\text{Li}_x\text{Si}}}{1 + \nu} \left[\mathbf{D}^E + \frac{\nu}{1 - 2\nu} \mathbf{D}_{kk}^E \mathbf{I} \right]. \quad (2)$$

Here, $\dot{\boldsymbol{\tau}}^v$ is the Jaumann rate of the Kirchhoff stress $\boldsymbol{\tau}$. $E_{\text{Li}_x\text{Si}}$ and ν denote the Young's modulus and Poisson's ratio, respectively, and both vary linearly with normalized Li concentration C from 160 GPa to 40 GPa and from 0.24 to 0.22 respectively. The plastic stretch rate \mathbf{D}^P can be determined by classical J_2 flow rule and the yield strength σ_Y is taken to be 1 GPa (Sethuraman et al., 2010). Based on the abovementioned framework, the lithiation-induced deformation field can be obtained by solving boundary-value problems numerically via finite element method.

3. Stress evolution in a-Si particle anodes

3.1. Stress evolution in a solid a-Si particle: chemo-mechanical simulations

We first consider a pristine solid a-Si particle with an initial radius R_0 . Position of a material point in the a-Si particle is specified by a radius R ($0 \leq R \leq R_0$) in the unlithiated state. Fig. 2(a) plots the radial distribution of normalized lithium concentration C at five representative stages during the two-step lithiation. In the first step, the lithiation advances via the two-phase mechanism, with a sharp reaction interface (represented by a step function of $C = 0$ (pristine) ahead of reaction front and $C = 0.67$ ($\text{Li}_{2.5}\text{Si}$) in the wake, as shown in Fig. 2(a)) migrating inward. In the second step, the lithium concentration remains a uniform profile and gradually ramps up from 0.67 to 1 ($\text{Li}_{3.75}\text{Si}$), as pointed out by recent ab initio calculations (Cubuk and Kaxiras, 2014).

Fig. 2(b)–(f) shows the stress evolution during the two-step lithiation by plotting the radial distribution of three stress components (von Mises stress σ_{vM} , hoop stress σ_θ and radial stress σ_r , respectively, normalized by the yield stress of a-Si, σ_Y) at the five representative stages defined in Fig. 2(a). In the first step of lithiation (Fig. 2(b) and (c)), the unlithiated core of the a-Si particle is under increasing hydrostatic compression as the lithiation advances. The hydrostatic nature of stress results in a zero von Mises stress in the unlithiated core. At the reaction front, the constraint from the inner unlithiated core acts against the lithiation-induced volume expansion of the outer partially lithiated $\text{Li}_{2.5}\text{Si}$ phase. As a result, the $\text{Li}_{2.5}\text{Si}$ phase at the reaction front is under compressive stresses σ_θ and σ_r ; and the resulting von Mises stress readily exceeds the yielding strength, causing yielding of the partially lithiated a-Si phase on the reaction front. In the outer partially lithiated shell, the stress state is highly triaxial. The radial stress σ_r in the $\text{Li}_{2.5}\text{Si}$ shell is compressive, and gradually decreases to zero from the reaction front to the free outer surface of the particle. Due to the “pushing-out” effect (Huang et al., 2013), the $\text{Li}_{2.5}\text{Si}$ shell undergoes elastic unloading and the hoop stress σ_θ gradually becomes tensile in the shell and eventually reaches σ_Y at the external surface of the particle. Such a triaxial stress state leads to the complete yielding of the whole $\text{Li}_{2.5}\text{Si}$ shell (i.e., $\sigma_{vM} = \sigma_Y$). Stress profile in the a-Si particle during the first step is very similar to that in a c-Si particle during lithiation, with the similarity resulting from the reaction-controlled two-phase lithiation (Liu et al., 2011, 2012c; Yang et al., 2012; Zhao et al., 2012b).

In the second step of lithiation, the most salient feature of stress evolution is the stress relaxation associated with the advance of lithiation stage, which is absent in the lithiation of c-Si. As evident from Fig. 2(d)–(f), the amplitudes of both σ_θ

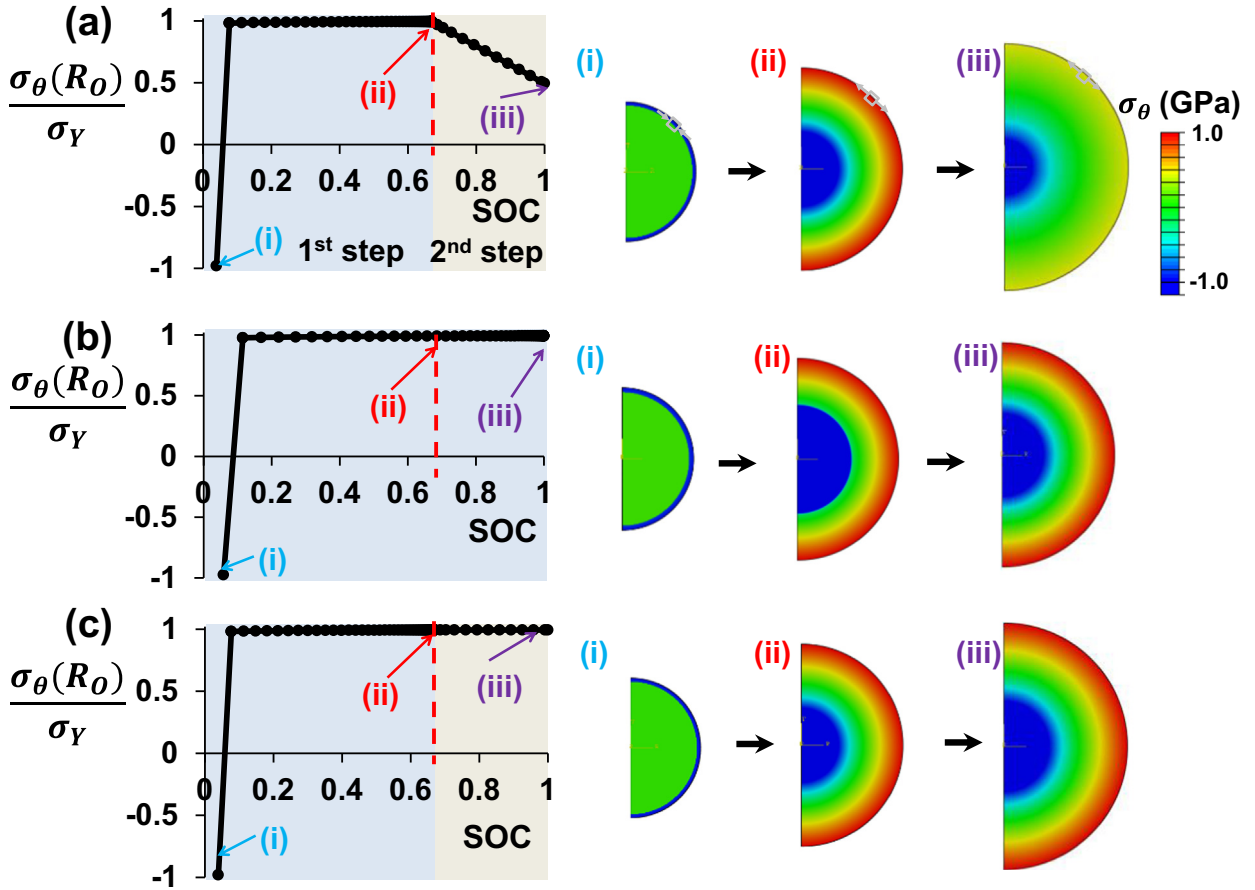


Fig. 3. Evolution of hoop stress at the surface layer of the particle undergoing the real two-step lithiation process and two hypothetical lithiation scenarios. (a) Two-step lithiation mechanism with elastic softening. Hoop stress linearly drops with increasing SOC during the second step of lithiation. Representative snapshots (i)–(iii) are shown to reveal hoop stress profiles at representative stages. (b) One-step lithiation mechanism, similar to that in c-Si, with elastic softening. The hoop stress remains to be σ_Y until the completion of lithiation. (c) Two-step lithiation mechanism with constant elastic modulus. No relaxation of hoop stress occurs.

and σ_r decrease significantly upon further lithiation, which leads to the drop of von Mises stress level in the particle. In particular, the tensile hoop stress at the outer surface of the a-Si particle contributes the most to the driving force for anode fracture (Liu et al., 2012c; Zhao et al., 2012b). Results in Fig. 2(d)–(f) show that the amplitude of such a stress decreases from σ_Y at the end of the first step (Fig. 2(d)), to $0.76\sigma_Y$ when the particle is lithiated to Li_3Si (Fig. 2(e)), and finally to $0.49\sigma_Y$ at fully lithiated state of $\text{Li}_{3.75}\text{Si}$ (Fig. 2(f)). In other words, the two-step lithiation can effectively mitigate the lithiation-induced stress, the key mechanism for the increased critical size of a-Si nanoparticle anodes in comparison with their c-Si counterparts. A more quantitative comparison of the critical anode size between a-Si and c-Si will be given later.

To further reveal the underlying mechanism of the unique stress relaxation during the second step of lithiation, we compare the evolution of the hoop stress σ_θ at the outer surface of the a-Si particle ($R = R_0$) during real lithiation process and under another two hypothetical lithiation scenarios. Note there are two salient features associated with the real lithiation process of a-Si: (i) the real lithiation process occurs via a two-step lithiation mechanism and (ii) the elastic modulus of the lithiated silicon decreases linearly with lithium concentration. Fig. 3(a) plots σ_θ at $R = R_0$ as a function of the state of charge (SOC) in real lithiation process. Here the state of charge (SOC) is defined as: $\text{SOC} = C(R_0^3 - r_f^3)/R_0^3$. In the first step of lithiation, $C = 0.67$ and r_f decreases from R_0 to 0, giving $\text{SOC} = 0$ for un lithiated particle and $\text{SOC} = 0.67$ at the end of the first step. In the second step of lithiation, $r_f = 0$ while normalized concentration C ramps from 0.67 to 1 upon charging, eventually leading to $\text{SOC} = 1$ at full lithiation of the particle. In Fig. 3(a), the onset of lithiation from the outer surface poses a dilational strain due to lithium insertion. Owing to the constraint from the inner un lithiated core, significant compressive stress develops at the outer surface and reaches material yielding in compression, i.e., $\sigma_\theta = -\sigma_Y$, at $R = R_0$. As the sharp reaction front advances toward the center of the particle, lithiation-induced swelling pushes out the $\text{Li}_{1.5}\text{Si}$ phase behind the reaction front and thus causes elastic unloading of compression, then tensile elastic loading and finally tensile plastic yielding (i.e., $\sigma_\theta = \sigma_Y$, at

$u_i = 0.0035 - 5.6e^{-6} + 1.09e^{-9}w^2 - 1.2e^{-14}$) in the hoop direction of the outer surface. The tensile plastic yielding maintains until the end of the first lithiation step (SOC = 0.67). In the second step of lithiation ($0.67 < \text{SOC} \leq 1$), hoop stress at the outer surfaces decreases linearly from σ_Y to $0.49\sigma_Y$ at full lithiation (SOC = 1). Fig. 3(b) plots the evolution of the hoop stress at the outer surface of the same a-Si particle undergoing a hypothetical one-step two-phase lithiation process, similar to that in a c-Si particle. The elastic modulus of lithiated silicon is still taken to be linearly dependent on lithium concentration as in real lithiation process. While the initial transition from compressive plastic yielding to tensile plastic yielding is the same as in Fig. 3(a), the tensile hoop stress at the outer surface remains as high as σ_Y upon completion of full lithiation. In other words, no stress relaxation occurs. Fig. 3(c) further plots such a stress evolution for another hypothetical scenario, in which the a-Si particle undergoes the same two-step lithiation as in the real scenario but the elastic modulus of the lithiated silicon is assumed to be independent of the lithium concentration (i.e., 160 GPa for all Li–Si phases). It is shown that the high hoop stress at the outer surface is not relaxed even though the a-Si particle is lithiated through a two-step process. The above comparison between the real and two hypothetical scenarios suggests that the two-step lithiation as well as the lithiation-induced elastic softening of a-Si are two key underlyings for the stress relaxation during lithiation of a-Si.

3.2. Stress evolution in a solid a-Si particle: validation by theoretical analysis

As an effort to validate the simulation results shown above, we next present a theoretical analysis of the lithiation-induced stress field in a solid a-Si particle undergoing two-step lithiation. The stress field can be calculated by a theoretical model considering concurrent lithiation and plasticity (Jia and Li, 2015; Zhao et al., 2012b). We consider a pristine solid a-Si particle with an outer radius R_0 as the reference state. In the reference configuration (i.e., unlithiated state, time $t=0$), a material point in the a-Si particle is located at the position with a radius R ($0 \leq R \leq R_0$). After lithiation begins ($t > 0$), lithiation-induced deformation drives this material point to move to a new position with a radius $r(R, t)$ in the current configuration. The reaction front at time t is characterized by its radius $r_f(t)$ in the current configuration. The outer radius $r_0(R_0, t)$ of the particle at time t increases due to lithiation. In our theoretical mechanistic model, the reference coordinate R is used as an independent variable to describe the stress field under two-step lithiation. During the first step, the deformed position $r(R, t)$ is given by

$$r(R, t) = \begin{cases} R & (R \leq r_f) \\ [r_f^3 + 3(R^3 - r_f^2)]^{1/3} & (r_f < R \leq R_0) \end{cases} \quad (3)$$

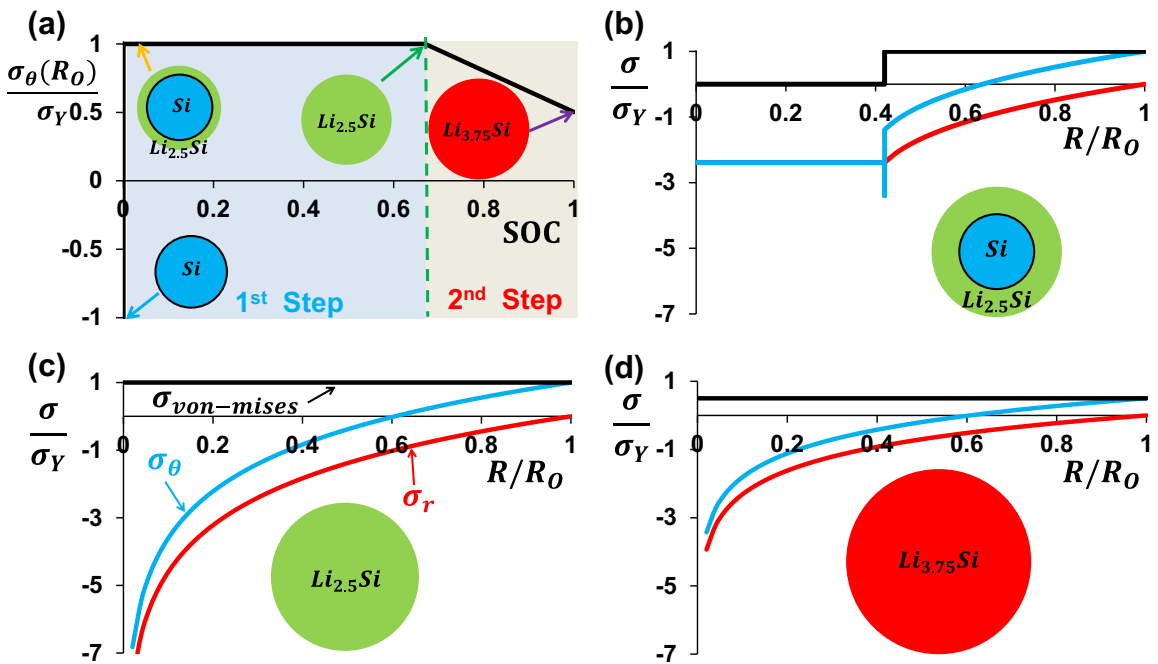


Fig. 4. Theoretical results of an a-Si particle undergoing two-step lithiation. (a) Hoop stress evolution at the particle surface ($R = R_0$) as a function of the state of charge (SOC). The plastic yielding during the first step and the linear decreasing of hoop stress owing to elastic softening during the second step are captured by the theoretical model. Insets illustrate the representative stages. Stress distributions (e.g., σ_r , σ_θ and σ_{vM}) in the whole particle are plotted at (b) an intermediate stage with $r_f/R_0 = 0.42$, (c) the start of second step (SOC = 0.67) and (d) end of second step (SOC = 1). The theoretical prediction shows remarkable agreement with the finite element modeling results shown in Fig. 2 and Fig. 3.

It is worth noting that the elastic deformation is ignored in this formulation because it is trivial compared with the finite-strain plastic deformation during lithiation process. Eq. (3) fully describes the lithiation-induced deformation field because all strain measures can be derived from it.

In the first lithiation step ($0 \leq \text{SOC} \leq 0.67$), consider true strain rate calculated from Eq. (3) and follow the theoretical framework developed by Zhao et al. (2012b), the Cauchy stress distribution within the lithiated particle is obtained

$$\sigma_r = \begin{cases} 2\sigma_Y \log(r/r_0) (r > r_f) \\ 2\sigma_Y \log(r_f/r_0) (r \leq r_f) \end{cases} \tag{4}$$

$$\sigma_\theta = \begin{cases} \sigma_Y + 2\sigma_Y \log(r/r_0) (r > r_f) \\ -\sigma_Y + 2\sigma_Y \log(r_f/r_0) (r = r_f) \\ 2\sigma_Y \log(r_f/r_0) (r < r_f) \end{cases} \tag{5}$$

Again, r denotes the position of a material point in lithiated particle at time t and is given by Eq. (3), r_f and r_0 represent the radii of the sharp reaction front and the particle outer surface at time t , respectively. Eqs. (4) and (5) can characterize the evolution of stress fields as a function of time t .

Given that SOC increases monotonically as time t increases, we can readily study the evolution of stress field in terms of SOC which directly relates the stress distribution to its corresponding lithiation stage. At the beginning of the lithiation

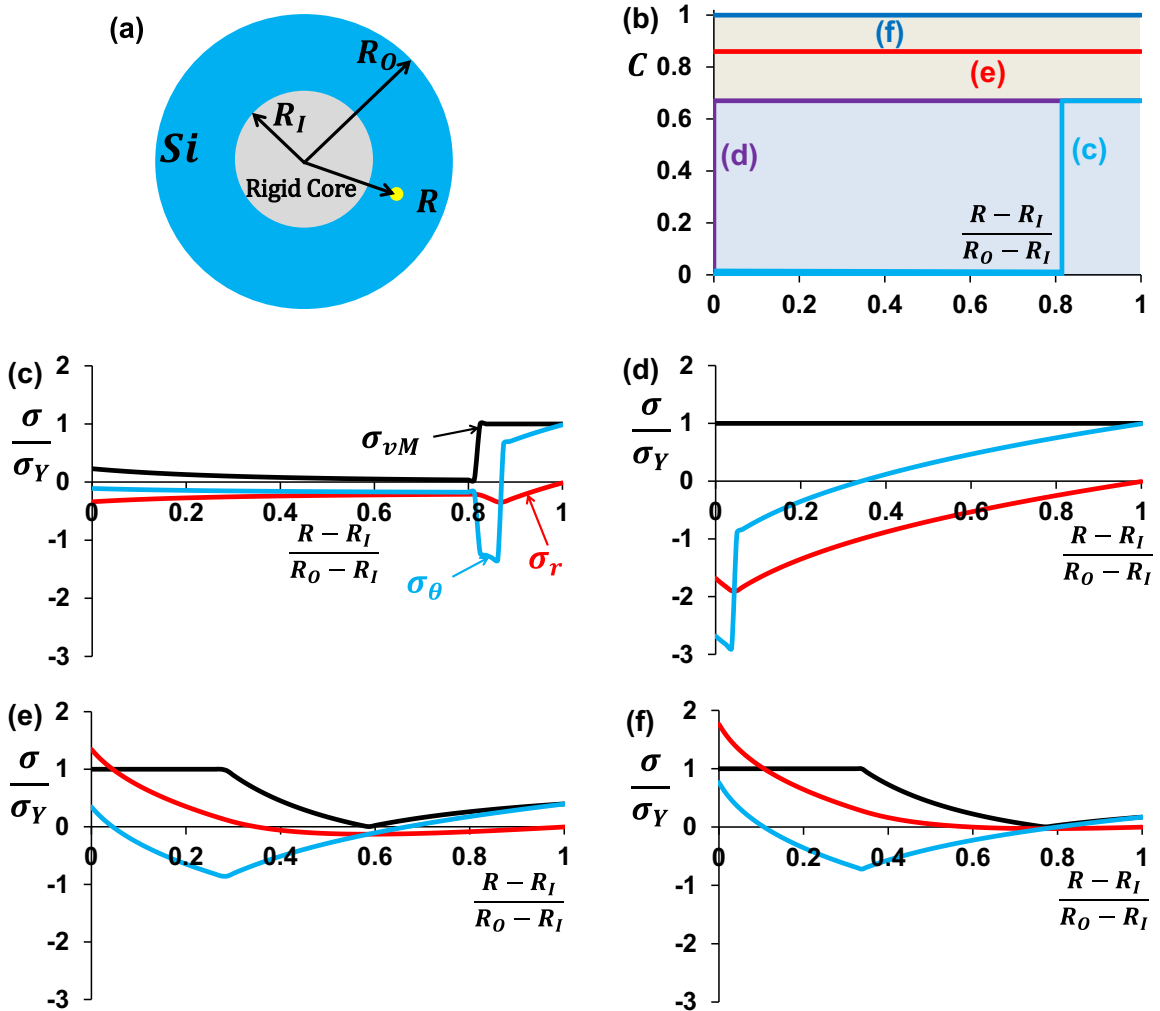


Fig. 5. Stress evolution in a hollow a-Si particle supported by an inner rigid core during the two-step lithiation. (a) Schematic of the hollow particle, with R_I being the inner radius, R_O the outer radius and R the distance from an element to the center, in the unlithiated state. (b) Representative Li profiles C along the radial direction are plotted as a function of $(R - R_I)/(R_O - R_I)$. (c) and (d) Stress distributions (σ_{vM} , σ_θ , σ_r) in the first step of lithiation. (e) and (f) Stress distribution in the second step of lithiation. Compared with that in a solid a-Si particle, hoop stress is further released because of the compression induced by the inner rigid core.

(SOC → 0), the reaction front is right on the particle surface, that is, $r_f=r_0$. Note that in Eq. (3), the hoop stress at the reaction front is given by $\sigma_\theta = -\sigma_Y + 2\sigma_Y \log\left(\frac{r_f}{r_0}\right)$. Therefore, at SOC → 0, we have

$$\sigma_\theta(R_0, \text{SOC}) = -\sigma_Y \quad (\text{SOC} = 0) \tag{6}$$

Subsequently, as the reaction front migrates towards the center of the particle, the material elements on the surface are pushed outward, being part of the $\text{Li}_{2.5}\text{Si}$ shell. As indicated by Eq. (5), the hoop stress within the lithiated shell is given by $\sigma_\theta = \sigma_Y + 2\sigma_Y \log\left(\frac{r}{r_0}\right)$. Therefore, hoop stress at the particle surface is

$$\sigma_\theta(R_0, \text{SOC}) = \sigma_Y, \quad (0 < \text{SOC} \leq 0.67) \tag{7}$$

During the second step of lithiation, inserted Li atoms uniformly distribute in the anode particle (Cubuk and Kaxiras, 2014). As a result, the anode swells uniformly, without affecting the elastic and plastic strain profiles, i.e. $\epsilon_{ij}^e(R, \text{SOC}) = \epsilon_{ij}^e(R, 0.67)$ and $\epsilon_{ij}^p(R, \text{SOC}) = \epsilon_{ij}^p(R, 0.67)$ with $0.67 \leq \text{SOC} \leq 1$, which is in agreement with the finite element modeling results. Moreover, as aforementioned, the stiffness of Li_xSi linearly decreases from 79.6 GPa to 40GPa as x increases from 2.5 to 3.75 (Yang et al., 2012). Such stiffness softening reduces the stress level to the elastic region during the second step. According to linear elasticity, it is obtained that

$$\sigma_r(R, \text{SOC}) = \frac{E_{\text{Li}_x\text{Si}}}{(1+\nu)(1-2\nu)} [(1-\nu)\epsilon_r^e(R, 0.67) + 2\nu\epsilon_\theta^e(R, 0.67)] \tag{8}$$

and

$$\sigma_\theta(R, \text{SOC}) = \frac{E_{\text{Li}_x\text{Si}}}{(1+\nu)(1-2\nu)} [\epsilon_\theta^e(R, 0.67) + \nu\epsilon_r^e(R, 0.67)], \tag{9}$$

with $0.67 \leq \text{SOC} \leq 1$. Considering the negligible change of Poisson’s ratio during lithiation, the hoop and radial stresses depends linearly on the Young’s modulus $E_{\text{Li}_x\text{Si}}$ during the second step of lithiation. Therefore, it is concluded that $\sigma_\theta(R, \text{SOC}) = \Omega\sigma_\theta(R, 0.67)$ and $\sigma_r(R, \text{SOC}) = \Omega\sigma_r(R, 0.67)$ for $0.67 \leq \text{SOC} \leq 1$, where $\Omega = \frac{E_{\text{Si}}(1-\text{SOC}) + E_{\text{Li}_{3.75}\text{Si}}\text{SOC}}{E_{\text{Li}_{2.5}\text{Si}}}$. The stress distribution in the particle during the second step of lithiation ($0.67 < \text{SOC} \leq 1$) is then given by

$$\sigma_r = 2\Omega\sigma_Y \log(r/r_0) \tag{10}$$

$$\sigma_\theta = \Omega\sigma_Y [1 + 2 \log(r/r_0)], \tag{11}$$

Specifically, the hoop stress at particle surface during the second step can be calculated from Eq. (11)

$$\sigma_\theta(R_0, \text{SOC}) = \Omega\sigma_Y, \quad (0.67 \leq \text{SOC} \leq 1) \tag{12}$$

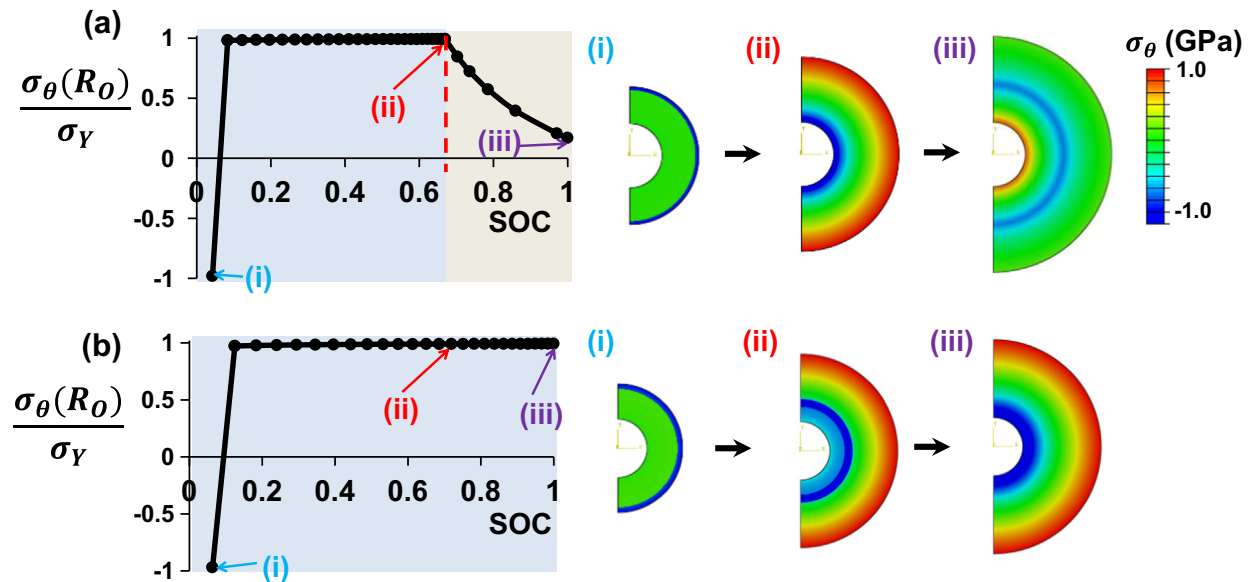


Fig. 6. Evolution of hoop stress at the surface layer of the hollow a-Si particle undergoing (a) real two-step lithiation and (b) hypothetical one-step two-phase lithiation. Direct comparison reveals that the second step of lithiation mitigates the high tensile stress at the surface layer.

Evolution of hoop stress on the particle surface at various lithiation stages is fully captured by Eqs. (6), (7) and (12). The result is summarized in Fig. 4(a), which agrees well with the finite element modeling results (Fig. 3(a)). The theoretical model neglects the elastic deformation in the wake of the reaction front, which results in an abrupt change of hoop stress from $-\sigma_Y$ to σ_Y in Fig. 4(a) after the onset of lithiation. Nonetheless, such a difference between theoretical prediction and finite element results plays a trivial role in determining the fracture behavior of the a-Si particle at the later stage of lithiation.

Based on stress profiles given by Eqs. (4)–(5) and (10)–(11), Fig. 4(b) plots the radial distribution of the stress field at an intermediate stage in the first step of lithiation ($r_f/R_0=0.42$, same stage as in Fig. 2(c)); Fig. 4(c) and (d) plots the radial distribution of the stress field at the beginning and the end of the second step of lithiation (i.e., SOC = 0.67 and 1), respectively. The theoretical prediction in Fig. 4(b)–(d) shows remarkable agreement with the finite element modeling results in Fig. 2(c), (d) and (f). The above theoretical analysis offers not only strong evidence to validate the finite element modeling results but also a mechanistic understanding of the stress evolution during the two-step lithiation of a solid a-Si particle. Our theoretical model reveals that, during the second lithiation step, all plastic strains ϵ_{ij}^p and elastic strains ϵ_{ij}^e remain unchanged (i.e., $\dot{\epsilon}_{ij}^p=\dot{\epsilon}_{ij}^e=0$), in response to the homogeneous volumetric expansion. As a result, the lithiated Si particle deforms within the elastic behavior regime and thus the linear lithiation-induced elastic softening leads to the linear drop of all stresses in the second step.

3.3. Stress evolution in a hollow a-Si particle

Recently, hollow nanostructured silicon anodes attract increasing attention due to their improved electric conductivity and better mechanical integrity during charging/discharging cycles (Chen et al., 2012; Kim et al., 2008; Liu et al., 2012a; Magasinski et al., 2010; Yan et al., 2013; Yao et al., 2011). Such hollow silicon anodes are often synthesized via deposition on the surface of an inner core (e.g., SiO_2 , Fig. 5(a)), which in turn acts as mechanical support for the hollow silicon anodes.

We next carry out the similar chemo-mechanical modeling as that for the solid a-Si particle to understand the effect of two-step lithiation on the stress evolution in such a hollow a-Si particle. Given that the elastic modulus of the inner core (e.g., SiO_2) is about 10 times as that of the lithiated silicon, it is reasonable to regard the inner core to be rigid, so that the inner surface of the hollow a-Si particle is constrained and cannot deform. The pristine hollow a-Si particle has an inner radius R_I and an outer radius R_O . We present the simulation results in terms of the radial coordinate R (distance from the center to a material point in pristine particle) in the reference state. Fig. 5(b) plots the radial distribution of normalized lithium concentration C at four representative stages during the two-step lithiation. Fig. 5(c)–(f) plots the radial distribution of three normalized stress components (σ_{VM}/σ_Y , σ_θ/σ_Y and σ_r/σ_Y , respectively) at these four stages. While the stress distribution and evolution during the first step of lithiation (e.g., Fig. 5(c) and (d)) are rather similar to those in a solid a-Si particle (e.g., Fig. 2(b)–(d)), the stress evolution during the second step of lithiation shows different feature from its solid counterpart. As shown in Fig. 5(e) and (f), once the reaction front hits the inner surface (i.e., $\frac{R-R_I}{R_O-R_I}=0$), the second step of lithiation sets in. The hollow particle tends to swell homogeneously in response to the uniform lithiation in the second step.

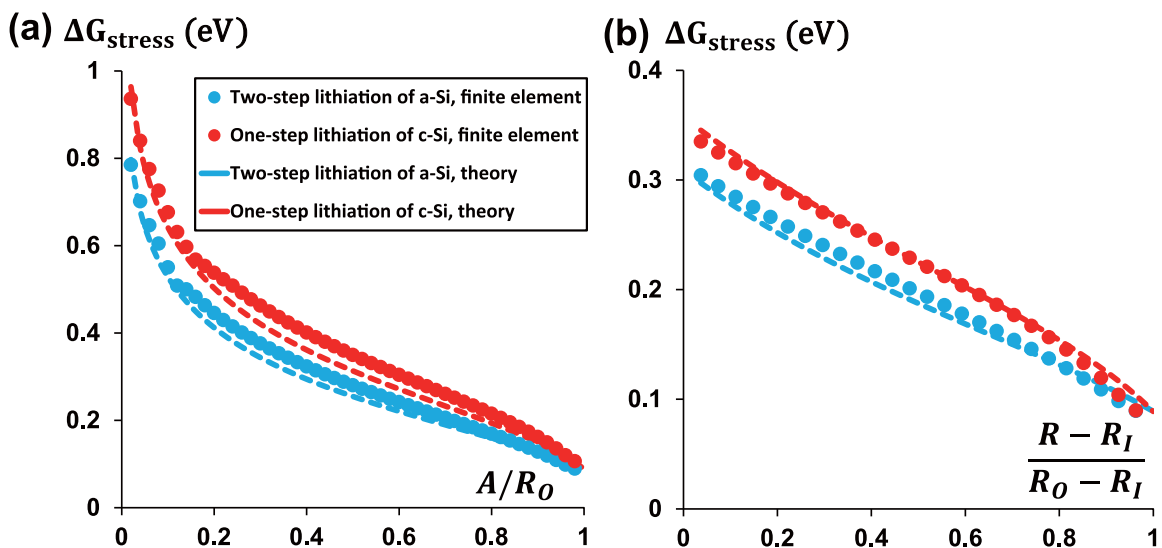


Fig. 7. Stress-modulated energy barrier for lithiation reaction is plotted as a function of lithiation front position in (a) solid a-Si (blue dots) and c-Si (red dots) particles and (b) hollow ones. Theoretical results (dashed lines) are also shown to benchmark the finite element modeling results. (For interpretation of the references to color in this figure legend, the reader is referred to the web version of this article.)

But the inner rigid core confines the outward radial expansion of the inner surface by applying a hydrostatic state of tension at the inner surface, causing a transition of radial and hoop stresses from compressive to tensile near the inner surface. The part near the free outer surface of the particle is hardly affected by the constraint at the inner surface. As a result, elastic softening of lithiated silicon results in effective elastic unloading, causing tensile hoop stress near the outer layer to drop as the second-step of lithiation advances.

Fig. 6(a) plots the evolution of the hoop stress at the outer surface of the hollow a-Si particle as a function of SOC in real lithiation process, which shows the similar relaxation during the second step of lithiation. Different from the linear relaxation of the hoop stress in a solid a-Si particle (e.g., Fig. 3(a)), the relaxation of the hoop stress in a hollow a-Si particle is nonlinear. This can be understood by the additional mechanical constraint of the rigid inner core, which poses further compression of the layer near the outer surface in the hoop direction, and thus in turn leads to more unloading of the tensile hoop stress. For example, at the end of full lithiation, the hoop stress in the outer surface of the hollow a-Si particle drops to $0.17\sigma_Y$, much lower than the final hoop stress of $0.49\sigma_Y$ in the solid a-Si particle. On the other hand, as revealed by the theoretical formulation, the linear stress relaxation for a solid a-Si particle results from vanishing strain increments $\dot{\epsilon}_{ij}^p$ and $\dot{\epsilon}_{ij}^e$ in response to homogeneous volume expansion. The existence of inner rigid core inside a hollow a-Si particle leads to heterogeneous volume expansion, causing non-zero elastic strain increments $\dot{\epsilon}_{ij}^e$ near the outer surface. Consequently, the combination of linear elastic modulus softening and changing elastic strains at outer surface results in the nonlinear drop.

Fig. 6(b) plots the evolution of the hoop stress at the outer surface of the hollow a-Si particle as a function of SOC for the hypothetical scenario of one-step two-phase lithiation process. Similar with the hypothetical case of its solid counterparts (Fig. 3(b)), the hoop stress at the outer surface of the particle remains as σ_Y until the completion of lithiation without stress relaxation, further suggesting the crucial role of two-step lithiation and elastic softening in mitigating the lithiation-induced fracture of a-Si anodes.

4. Reaction-induced fracture during two-phase lithiation of a solid a-Si particle

Next, we study the influence of the two-step lithiation of an a-Si particle on its lithiation-induced fracture as well as lithiation kinetics. Existing evidence suggests that the reaction-induced fracture of an a-Si particle is mainly caused by the tensile hoop stress generated near the particle surface during the lithiation. As revealed above, in the second step of lithiation, the particle expands homogeneously and the tensile hoop stress keeps decreasing due to material elastic softening. Therefore, it is reasonable to conclude that the particle may only fracture due to the stress generated in the first-step lithiation, which was also implied by recent ab initio calculations (Cubuk and Kaxiras, 2014). Dimensional analysis dictates the driving force for the propagation of a pre-existing crack in a $\text{Li}_{2.5}\text{Si}$ spherical particle of radius r_0 takes the form of

(Zhao et al., 2012b)

$$G = Z \frac{\sigma_Y^2}{E_{\text{Li}_{2.5}\text{Si}}} r_0 \quad (13)$$

where Z is a dimensionless parameter on the order of unity. For example, under two-phase lithiation, it has been reported $Z \sim 0.91$ for a particle with a precrack of a modest crack length (Zhao et al., 2012b). Fracture occurs when the driving force for crack propagation exceeds the fracture energy of the particle, Γ . Therefore, a critical particle size r_0^{cr} can be determined, above which the particle is subject to lithiation-induced fracture, given by

$$r_0^{\text{cr}} = \frac{E_{\text{Li}_{2.5}\text{Si}} \Gamma}{Z \sigma_Y^2} \quad (14)$$

Taking $Z = 1$, $\Gamma = 7\text{J/m}^2$ (Pharr et al., 2013), $E_{\text{Li}_{2.5}\text{Si}} = 79.6\text{GPa}$ and $\sigma_Y = 1\text{GPa}$ (Sethuraman et al., 2010), we find a critical radius of the $\text{Li}_{2.5}\text{Si}$ particle at the end of the first step of lithiation of $r_0^{\text{cr}} = 557.2\text{nm}$. The corresponding critical initial radius of the pristine a-Si particle is thus $R_0^{\text{cr}} = 386.3\text{nm}$, which agrees reasonably well with the reported value of 435nm in experiments (McDowell et al., 2013a).

The critical radius of a c-Si particle at full lithiation can be calculated in a similar fracture mechanics model, so that $r_0^{\text{cr}} = \frac{E_{\text{Li}_{3.75}\text{Si}} \Gamma}{Z \sigma_Y^2} = 280\text{nm}$. The corresponding critical radius of the pristine c-Si particle is then $R_0^{\text{cr}} = 176.4\text{nm}$. This estimation is much larger than the reported value of 75nm for c-Si particles in literature (Lee et al., 2012; McDowell et al., 2013a). Such a discrepancy can be attributed to anisotropic lithiation nature of the c-Si particle, which is not considered in the fracture mechanics model (Liang et al., 2013). Nonetheless, the theoretical prediction above offers quantitative insight for the significant difference in critical sizes of a-Si and c-Si particles observed in recent experiments, and further reveals the crucial role of two-step lithiation and elastic softening on the mechanical durability of a-Si anodes.

5. Effect of two-step lithiation on lithiation kinetics

Researches on lithiation kinetics have been performed for c-Si anodes. Experimental measurements of reaction velocity in solid c-Si particles reveal that the reaction front slows down as it progresses into the solid particles (McDowell et al., 2012). Existing theoretical studies show that lithiation-induced stress field could impede the lithiation reaction (Grantab and Shenoy, 2012). A recent theoretical model accounting for concurrent lithiation and plasticity (Zhao et al., 2012b) shows that the evolving stress field across the reaction front acts as an energy barrier for lithiation reaction and retards the velocity of the reaction front in c-Si. The stress-induced energy barrier for lithiation reaction is given by

$$\Delta G_{\text{stress}} = \frac{1}{\eta} \left[\sigma_m^{\text{Si}} \Omega^{\text{Si}} - \sigma_m^{\text{Li}_\eta\text{Si}} \Omega^{\text{Li}_\eta\text{Si}} \right] \quad (15)$$

where Ω^{Si} and $\Omega^{\text{Li}_\eta\text{Si}}$ represent the atomic volume of Si and Li_ηSi , respectively, and σ_m^{Si} and $\sigma_m^{\text{Li}_\eta\text{Si}}$ denote the mean stress in remaining un lithiated silicon and the mean stress on the lithiation front, respectively. The higher energy barrier ΔG_{stress} , the lower the driving force for lithiation reaction, and thus the slower migration of the reaction front.

Recent experiments show that the lithiation reaction in a-Si proceeds approximately at a constant velocity and does not slow down as much as in the c-Si case (McDowell et al., 2013a). Such a difference in lithiation kinetics is speculated to be due to the difference in the evolution of lithiation-induced stress, however there lacks quantitative evidence so far to support this speculation. To address this issue, we next calculate the stress-induced energy barrier for lithiation reaction in a solid a-Si particle undergoing a two-step lithiation. The spherical symmetry of the lithiation process of the a-Si particle leads to a mean stress $\sigma_m = \frac{1}{3}(\sigma_r + 2\sigma_\theta)$. Substituting Eqs. (4) and (5) into Eq. (15) gives the stress-induced energy barrier for lithiation reaction

$$\Delta G_{\text{stress}} = \frac{2\sigma_Y}{\eta} \left[(\Omega^{\text{Li}_\eta\text{Si}} - \Omega^{\text{Si}}) \log\left(\frac{r_0}{r_f}\right) + \frac{1}{3} \Omega^{\text{Li}_\eta\text{Si}} \right] \quad (16)$$

The effect of two-step lithiation on the lithiation kinetics of a-Si can be demonstrated by comparing the stress-induced energy barriers ΔG_{stress} for $\eta = 2.5$ (the case corresponding to the end of the first step of the real two-step lithiation process of a-Si) and $\eta = 3.75$ (the case corresponding to the end of the one-step lithiation process of c-Si) in Eq. (11), respectively. Fig. 7(a) shows such a comparison of stress-induced energy barriers as a function of the normalized location of lithiation front r_f/R_0 . Here $\Omega^{\text{Li}_{2.5}\text{Si}}/\Omega^{\text{Si}}=3$ and $\Omega^{\text{Li}_{3.75}\text{Si}}/\Omega^{\text{Si}}=4$. σ_Y is taken to be 1GPa (Sethuraman et al., 2010) and $\Omega_{\text{Si}}=2.9 \times 10^{-29}\text{m}^3$ (Zhao et al., 2011). At the onset of lithiation at the outer surface of the particle (i.e., $\frac{r_f}{R_0}=1$), ΔG_{stress} for the two cases are comparable. As the lithiation proceeds toward the center of the particle, ΔG_{stress} increases, suggesting that lithiation-induced stress poses increasing energy barrier for lithiation reaction. However, as the lithiation proceeds inward, ΔG_{stress} due to a two-step lithiation is always lower than that due to a one-step lithiation, for the same lithiation stage. The difference in ΔG_{stress} between the two cases increases modestly as the lithiation progresses. For example, at $\frac{r_f}{R_0}=0.02$, $\Delta G_{\text{stress}}=0.94\text{eV}$ for one-step lithiation and 0.79eV for two-step lithiation. Such a difference in ΔG_{stress} can be explained as follows. In the first step lithiation of a-Si, the partial lithiation by forming $\text{Li}_{2.5}\text{Si}$ results in less mechanical mismatch at the lithiation front and relatively lower stress level, and therefore lower energy barrier for lithiation reaction, compared with the one-step full lithiation of c-Si by forming $\text{Li}_{3.75}\text{Si}$. ΔG_{stress} can also be estimated from Eq. (15) using the stress fields obtained from finite element modeling results, which is also plotted in Fig. 7(a) and shows the similar trend as in theoretical prediction from Eq. (16). Note that for the hypothetical one-step lithiation of c-Si here is assumed to be isotropic, while in reality the lithiation of c-Si is anisotropic, which is expected to result in even higher lithiation-induced stress. Therefore, the comparison in Fig. 7(a) underestimates the difference in ΔG_{stress} for a-Si and c-Si. In other words, the stress-induced energy barrier in c-Si could be high enough to impede or even halt the lithiation reaction, while such an energy barrier in a-Si is modest without causing appreciable slowing down of the lithiation reaction.

The above comparison of the stress-induced energy barrier for lithiation reaction also holds for the case of hollow Si particles, as shown in Fig. 7(b). It is worth noting that the overall level of ΔG_{stress} for hollow Si particles is much lower than that for solid Si particles. For example, toward the end of the first step lithiation, ΔG_{stress} is only about 0.3eV for a hollow a-Si particle, less than half of ΔG_{stress} (0.79eV) for a solid a-Si particle. These results suggest that hollow Si particles can be more readily lithiated and less susceptible to stress-induced retardation of lithiation, which agrees with recent experimental observations (McDowell et al., 2013a; Yao et al., 2011) and chemo-mechanical modeling results (Jia and Li, 2015).

From a mechanics perspective, our calculation partially explains why the reaction front in a-Si does not slow as much as that in the c-Si case. However, the difference of lithiation kinetics between a-Si and c-Si may also be owing to other electrochemical aspects, which is beyond the scope of this work.

6. Summary and conclusions

In this work, we developed a chemo-mechanical modeling framework to study the lithiation of amorphous silicon. In our model, the first lithiation of amorphous silicon occurs via a two-step mechanism (Wang et al., 2013). The first step proceeds with the movement of a sharp interface separating the unlithiated a-Si phase and a partially lithiated phase $\text{Li}_{2.5}\text{Si}$ (Wang et al., 2013), and the phase interface moves towards the a-Si phase until the entire a-Si anode is partially lithiated to $\text{Li}_{2.5}\text{Si}$. Note that the Li concentration in the $\text{Li}_{2.5}\text{Si}$ phase remains a constant during the first step. Such a unique lithium concentration profile together with the existence of the sharp phase interface indicates a reaction-controlled lithiation mechanism. In the second step, further lithiation causes Li concentration in the partially lithiated phase to increase uniformly until full lithiation, i.e., from $\text{Li}_{2.5}\text{Si}$ to $\text{Li}_{3.75}\text{Si}$ (Cubuk and Kaxiras, 2014), dictated by a diffusion-controlled mechanism. In summary, amorphous silicon is lithiated via a two-step mechanism with the first step dominated by a reaction-controlled mechanism and the second step governed by a diffusion-controlled mechanism. Interestingly, it is worth noting that some recent continuum-scale simulations predict that the two mechanisms may coexist and interact in the first step, resulting in a non-uniform concentration distribution in the partially lithiated phase behind the phase interface (Cui et al., 2013a; Zhang et al., 2015). Further experimental and ab initio studies are needed to verify such a prediction.

Based on the two-step lithiation mechanism described above, we investigate the stress evolution in a-Si particles undergoing two-step lithiation. The two-step lithiation mechanism as well as the lithiation-dependent elastic softening leads to crucial consequences for fracture behavior and lithiation kinetics in a-Si anodes. Both finite element modeling and theoretical analysis reveal that the uniform distribution of Li during the second step of lithiation as well as the stiffness softening of lithiated silicon relaxes the stresses in the particle. The reduced stress level plays an important role in the lithiation kinetics and fracture behavior of a-Si particle. Compared with the c-Si case, the movement of reaction front in an a-Si particle experiences lower mechanical energy barrier; and the critical fracture size of a-Si particle is much higher than that of the c-Si particle, which agrees reasonably with experimental observations. Our findings shed fundamental insight into quantitative understanding about stress mitigation and its impact on battery performance in a-Si anodes, which may assist in the design of better lithium ion battery.

References

- Armand, M., Tarascon, J.M., 2008. Building better batteries. *Nature* 451, 652–657.
- Baggetto, L., Danilov, D., Notten, P.H.L., 2011. Honeycomb-structured silicon: remarkable morphological changes induced by electrochemical (de)lithiation. *Adv. Mater.* 23, 1563–1566.
- Berla, L.A., Lee, S.W., Ryu, I., Cui, Y., Nix, W.D., 2014. Robustness of amorphous silicon during the initial lithiation/delithiation cycle. *J. Power Sources* 258, 253–259.
- Bogart, T.D., Oka, D., Lu, X., Gu, M., Wang, C., Korgel, B.A., 2014. Lithium ion battery performance of silicon nanowires with carbon skin. *ACS Nano* 8, 915–922.
- Bower, A., Guduru, P., Sethuraman, V., 2011. A finite strain model of stress, diffusion, plastic flow, and electrochemical reactions in a lithium-ion half-cell. *J. Mech. Phys. Solids* 59, 804–828.
- Chan, C.K., Peng, H., Liu, G., McIlwrath, K., Zhang, X.F., Huggins, R.A., Cui, Y., 2008. High-performance lithium battery anodes using silicon nanowires. *Nat. Nanotechnol.* 3, 31–35.
- Chen, D., Mei, X., Ji, G., Lu, M., Xie, J., Lu, J., Lee, J.Y., 2012. Reversible lithium-ion storage in silver-treated nanoscale hollow porous silicon particles. *Angew. Chem. – Int. Ed.* 51, 2409–2413.
- Chen, Z., Wang, C., Lopez, J., Lu, Z., Cui, Y., Bao, Z., 2015. High-areal-capacity silicon electrodes with low-cost silicon particles based on spatial control of self-healing binder. *Adv. Energy Mater.*, 5.
- Cubuk, E.D., Kaxiras, E., 2014. Theory of structural transformation in lithiated amorphous silicon. *Nano Lett.* 14, 4065–4070.
- Cui, Z., Gao, F., Qu, J., 2013a. Interface-reaction controlled diffusion in binary solids with applications to lithiation of silicon in lithium-ion batteries. *J. Mech. Phys. Solids* 61, 293–310.
- Cui, Z., Gao, F., Qu, J., 2013b. Two-phase versus two-stage versus multi-phase lithiation kinetics in silicon. *Appl. Phys. Lett.*, 103.
- Goldman, J.L., Long, B.R., Gewirth, A.A., Nuzzo, R.G., 2011. Strain anisotropies and self-limiting capacities in single-crystalline 3D silicon microstructures: models for high energy density lithium-ion battery anodes. *Adv. Funct. Mater.* 21, 2412–2422.
- Grantab, R., Shenoy, V.B., 2012. Pressure-gradient dependent diffusion and crack propagation in lithiated silicon nanowires. *J. Electrochem. Soc.* 159, A584–A591.
- Gu, M., Yang, H., Perea, D.E., Zhang, J.G., Zhang, S., Wang, C.M., 2014. Bending-induced symmetry breaking of lithiation in germanium nanowires. *Nano Lett.* 14, 4622–4627.
- Haftbaradaran, H., Xiao, X., Verbrugge, M.W., Gao, H., 2012. Method to deduce the critical size for interfacial delamination of patterned electrode structures and application to lithiation of thin-film silicon islands. *J. Power Sources* 206, 357–366.
- Huang, S., Fan, F., Li, J., Zhang, S., Zhu, T., 2013. Stress generation during lithiation of high-capacity electrode particles in lithium ion batteries. *Acta Mater.* 61, 4354–4364.
- Jia, Z., Li, T., 2015. Stress-modulated driving force for lithiation reaction in hollow nano-anodes. *J. Power Sources* 275, 866–876.
- Karki, K., Epstein, E., Cho, J.H., Jia, Z., Li, T., Picraux, S.T., Wang, C., Cumings, J., 2012. Lithium-assisted electrochemical welding in silicon nanowire battery electrodes. *Nano Lett.* 12, 1392–1397.
- Key, B., Bhattacharyya, R., Morcrette, M., Seznec, V., Tarascon, J., Grey, C., 2009. Real-time NMR investigations of structural changes in silicon electrodes for lithium-ion batteries. *J. Am. Chem. Soc.* 131, 9239–9249.
- Key, B., Morcrette, M., Tarascon, J., Grey, C., 2011. Pair distribution function analysis and solid state NMR studies of silicon electrodes for lithium ion batteries: understanding the (de)lithiation mechanisms. *J. Am. Chem. Soc.* 133, 503–512.
- Kim, H., Han, B., Choo, J., Cho, J., 2008. Three-dimensional porous silicon particles for use in high-performance lithium secondary batteries. *Angew. Chem. – Int. Ed.* 47, 10151–10154.
- Lee, S.W., Lee, H.W., Ryu, I., Nix, W.D., Gao, H., Cui, Y., 2015. Kinetics and fracture resistance of lithiated silicon nanostructure pairs controlled by their mechanical interaction. *Nat. Commun.*, 6.
- Lee, S.W., McDowell, M.T., Berla, L.A., Nix, W.D., Cui, Y., 2012. Fracture of crystalline silicon nanopillars during electrochemical lithium insertion. *Proc. Natl. Acad. Sci. USA* 109, 4080–4085.

- Lee, S.W., McDowell, M.T., Choi, J.W., Cui, Y., 2011. Anomalous shape changes of silicon nanopillars by electrochemical lithiation. *Nano Lett.* 11, 3034–3039.
- Li, J., Dahn, J.R., 2007. An in situ X-ray diffraction study of the reaction of Li with crystalline Si. *J. Electrochem. Soc.* 154, A156–A161.
- Liang, W.T., Yang, H., Fan, F.F., Liu, Y., Liu, X.H., Huang, J.Y., Zhu, T., Zhang, S.L., 2013. Tough germanium nanoparticles under electrochemical cycling. *ACS Nano* 7, 3427–3433.
- Liu, N., Huo, K., McDowell, M.T., Zhao, J., Cui, Y., 2013. Rice husks as a sustainable source of nanostructured silicon for high performance Li-ion battery anodes. *Sci. Rep.*, 3.
- Liu, N., Wu, H., McDowell, M.T., Yao, Y., Wang, C., Cui, Y., 2012a. A yolk-shell design for stabilized and scalable Li-ion battery alloy anodes. *Nano Lett.* 12, 3315–3321.
- Liu, X., Wang, J., Huang, S., Fan, F., Huang, X., Liu, Y., Krylyuk, S., Yoo, J., Dayeh, S., Davydov, A., Mao, S., Picraux, S., Zhang, S., Li, J., Zhu, T., Huang, J., 2012b. In situ atomic-scale imaging of electrochemical lithiation in silicon. *Nat. Nanotechnol.* 7, 749–756.
- Liu, X.H., Zheng, H., Zhong, L., Huan, S., Karki, K., Zhang, L.Q., Liu, Y., Kushima, A., Liang, W.T., Wang, J.W., Cho, J.H., Epstein, E., Dayeh, S.A., Picraux, S.T., Zhu, T., Li, J., Sullivan, J.P., Cumings, J., Wang, C., Mao, S.X., Ye, Z.Z., Zhang, S., Huang, J.Y., 2011. Anisotropic swelling and fracture of silicon nanowires during lithiation. *Nano Lett.* 11, 3312–3318.
- Liu, X.H., Zhong, L., Huang, S., Mao, S.X., Zhu, T., Huang, J.Y., 2012c. Size-dependent fracture of silicon nanoparticles during lithiation. *ACS Nano* 6, 1522–1531.
- Lu, Z., Liu, N., Lee, H.W., Zhao, J., Li, W., Li, Y., Cui, Y., 2015. Nonfilling carbon coating of porous silicon micrometer-sized particles for high-performance lithium battery anodes. *ACS Nano* 9, 2540–2547.
- Luo, L., Yang, H., Yan, P., Travis, J.J., Lee, Y., Liu, N., Piper, D.M., Lee, S.H., Zhao, P., George, S.M., Zhang, J.G., Cui, Y., Zhang, S., Ban, C., Wang, C.M., 2015. Surface-coating regulated lithiation kinetics and degradation in silicon nanowires for lithium ion battery. *ACS Nano* 9, 5559–5566.
- Magasinski, A., Dixon, P., Hertzberg, B., Kvit, A., Ayala, J., Yushin, G., 2010. High-performance lithium-ion anodes using a hierarchical bottom-up approach. *Nat. Mater.* 9, 353–358.
- McDowell, M., Ryu, I., Lee, S., Wang, C., Nix, W., Cui, Y., 2012. Studying the kinetics of crystalline silicon nanoparticle lithiation with in situ transmission electron microscopy. *Adv. Mater.* 24, 6034–6041.
- McDowell, M.T., Lee, S.W., Harris, J.T., Korgel, B.A., Wang, C., Nix, W.D., Cui, Y., 2013a. In situ TEM of two-phase lithiation of amorphous silicon nanospheres. *Nano Lett.* 13, 758–764.
- McDowell, M.T., Lee, S.W., Nix, W.D., Cui, Y., 2013b. 25th anniversary article: understanding the lithiation of silicon and other alloying anodes for lithium-ion batteries. *Adv. Mater.* 25, 4966–4984.
- Obrovac, M.N., Christensen, L., 2004. Structural changes in silicon anodes during lithium insertion/extraction. *Electrochem. Solid State Lett.* 7, A93–A96.
- Pharr, M., Suo, Z., Vlassak, J.J., 2013. Measurements of the fracture energy of lithiated silicon electrodes of Li-ion batteries. *Nano Lett.* 13, 5570–5577.
- Pharr, M., Zhao, K., Wang, X., Suo, Z., Vlassak, J.J., 2012. Kinetics of initial lithiation of crystalline silicon electrodes of lithium-ion batteries. *Nano Lett.* 12, 5039–5047.
- Sethuraman, V.A., Chon, M.J., Shimshak, M., Srinivasan, V., Guduru, P.R., 2010. In situ measurements of stress evolution in silicon thin films during electrochemical lithiation and delithiation. *J. Power Sources* 195, 5062–5066.
- Shenoy, V.B., Johari, P., Qi, Y., 2010. Elastic softening of amorphous and crystalline Li–Si phases with increasing Li concentration: a first-principles study. *J. Power Sources* 195, 6825–6830.
- Soni, S.K., Sheldon, B.W., Xiao, X., Verbrugge, M.W., Ahn, D., Haftbaradaran, H., Gao, H., 2012. Stress mitigation during the lithiation of patterned amorphous Si islands. *J. Electrochem. Soc.* 159, A38–A43.
- Sun, C.F., Karki, K., Jia, Z., Liao, H., Zhang, Y., Li, T., Qi, Y., Cumings, J., Rubloff, G.W., Wang, Y., 2013. A beaded-string silicon anode. *ACS Nano* 7, 2717–2724.
- Takamura, T., Ohara, S., Uehara, M., Suzuki, J., Sekine, K., 2004. A vacuum deposited Si film having a Li extraction capacity over 2000 mAh/g with a long cycle life. *J. Power Sources* 129, 96–100.
- Tarascon, J.M., Armand, M., 2001. Issues and challenges facing rechargeable lithium batteries. *Nature* 414, 359–367.
- Wan, J., Kaplan, A.F., Jia, Z., Han, X., Chen, Y., Weadock, N.J., Faenza, N., Lacey, S., Li, T., Guo, J., Hu, L., 2014. Two dimensional silicon nanowalls for lithium ion batteries. *J. Mater. Chem. A*, 6051–6057.
- Wang, J.W., He, Y., Fan, F., Liu, X.H., Xia, S., Liu, Y., Harris, C.T., Li, H., Huang, J.Y., Mao, S.X., Zhu, T., 2013. Two-phase electrochemical lithiation in amorphous silicon. *Nano Lett.* 13, 709–715.
- Wang, J.W., Liu, X.H., Mao, S.X., Huang, J.Y., 2012. Microstructural evolution of tin nanoparticles during in situ sodium insertion and extraction. *Nano Lett.* 12, 5897–5902.
- Wang, X., Fan, F., Wang, J., Wang, H., Tao, S., Yang, A., Liu, Y., Chew, H.B., Mao, S.X., Zhu, T., Xia, S., 2015. High damage tolerance of electrochemically lithiated silicon. *Nat. Commun.* 6, 8417.
- Wu, H., Cui, Y., 2012. Designing nanostructured Si anodes for high energy lithium ion batteries. *Nano Today* 7, 414–429.
- Xu, R., Zhao, K., 2015. Mechanical interactions regulated kinetics and morphology of composite electrodes in Li-ion batteries. *Extrem. Mech. Lett.* <http://dx.doi.org/10.1016/j.eml.2015.10.004>.
- Yan, N., Wang, F., Zhong, H., Li, Y., Wang, Y., Hu, L., Chen, Q., 2013. Hollow porous SiO₂ nanocubes towards high-performance anodes for lithium-ion batteries. *Sci. Rep.*, 3.
- Yang, H., Fan, F., Liang, W., Guo, X., Zhu, T., Zhang, S., 2014. A chemo-mechanical model of lithiation in silicon. *J. Mech. Phys. Solids* 70, 349–361.
- Yang, H., Huang, S., Huang, X., Fan, F., Liang, W., Liu, X.H., Chen, L.Q., Huang, J.Y., Li, J., Zhu, T., Zhang, S., 2012. Orientation-dependent interfacial mobility governs the anisotropic swelling in lithiated silicon nanowires. *Nano Lett.* 12, 1953–1958.
- Yang, H., Liang, W., Guo, X., Wang, C.M., Zhang, S., 2015. Strong kinetics-stress coupling in lithiation of Si and Ge anodes. *Extrem. Mech. Lett.* 2, 1–6.
- Yang, Y., McDowell, M.T., Jackson, A., Cha, J.J., Hong, S.S., Cui, Y., 2010. New nanostructured Li₂S/silicon rechargeable battery with high specific energy. *Nano Lett.* 10, 1486–1491.
- Yao, Y., McDowell, M.T., Ryu, I., Wu, H., Liu, N., Hu, L., Nix, W.D., Cui, Y., 2011. Interconnected silicon hollow nanospheres for lithium-ion battery anodes with long cycle life. *Nano Lett.* 11, 2949–2954.
- Zhang, X., Lee, S.W., Lee, H.W., Cui, Y., Linder, C., 2015. A reaction-controlled diffusion model for the lithiation of silicon in lithium-ion batteries. *Extrem. Mech. Lett.* 4, 61–75.
- Zhao, K., Pharr, M., Hartle, L., Vlassak, J.J., Suo, Z., 2012a. Fracture and debonding in lithium-ion batteries with electrodes of hollow core-shell nanostructures. *J. Power Sources* 218, 6–14.
- Zhao, K., Pharr, M., Wan, Q., Wang, W.L., Kaxiras, E., Vlassak, J.J., Suo, Z., 2012b. Concurrent reaction and plasticity during initial lithiation of crystalline silicon in lithium-ion batteries. *J. Electrochem. Soc.* 159, A238–A243.
- Zhao, K., Wang, W.L., Gregoire, J., Pharr, M., Suo, Z., Vlassak, J.J., Kaxiras, E., 2011. Lithium-assisted plastic deformation of silicon electrodes in lithium-ion batteries: a first-principles theoretical study. *Nano Lett.* 11, 2962–2967.
- Zhu, T., 2015. Mechanics of high-capacity electrodes in lithium-ion batteries. *Chin. Phys. B* 25, 014601.